CCFE
CULHAM CENTRE FOR FUSION ENERGY

UK Atomic Energy Authority

UKAEA-CCFE-PR(25)301

C. Jones, Y.Andrew, T. Ashton-Key, F. Federici, T. Rhodes, E. Kim, R. Scannell

Spatio-Temporal Turbulence Dynamics over the MAST-U Edge Transport Barrier Evolution

Spatio-Temporal Turbulence Dynamics over the MAST-U Edge Transport Barrier Evolution

C. Jones, Y.Andrew, T. Ashton-Key, F. Federici, T. Rhodes, E. Kim, R. Scannell

This is a preprint of a paper submitted for publication in Nuclear Fusion Letter

Spatio-Temporal Turbulence Dynamics over the MAST-U Edge Transport Barrier Evolution

C. Jones[1,2], Y.Andrew[1], T. Ashton-Key[1], F. Federici[3], T. Rhodes[2], E. Kim[4,5], R. Scannell[3] and the MAST-U Team[3]

[1] Blackett Laboratory, Imperial College London, London SW7 2AZ, UK
[2] Department of Physics and Astronomy, University of California Los Angeles, Los Angeles, California 90095, USA
[3] United Kingdom Atomic Energy Authority, Culham Campus, Abingdon, Oxon OX14 3DB, United Kingdom
[4] Fluid and Complex System Research Centre, Coventry University, Coventry CV1 2TT, UK
[5] Nuclear Research Institute for Future Technology and Policy, Seoul National University, Seoul 08826, Korea

E-mail: ciaran.jones19@imperial.ac.uk

Abstract. Detailed results are presented from the first experimental study of self-regulation between plasma relative density fluctuations, $\tilde{n}_e$, and perpendicular velocity, $\tilde{v}_\perp$, over limit cycle oscillations (LCO) across the edge and near scrape-off layer (SOL) regions of the MAST-U spherical tokamak. The start of the dithering phase is preceded by the localisation of the emissivity at the magnetic null point. The L-H-mode-like transitions of the LCOs are characterised by a decrease in the mean $\tilde{n}_e$ and a narrowing of the probability density functions (PDF) due to plasma turbulence suppression. Sharp decreases in the $\tilde{n}_e$ skewness, $S_{\tilde{n}_e}$, are observed to routinely coincide with the start of the LCO in a narrow region of ($0.970 \leq \psi_N \leq 0.978$), corresponding to the location of the steepest pedestal pressure and $\bar{v}_\perp$ gradients. The decrease in $S_{\tilde{n}_e}$ during the LCOs in the regions closer to the SOL, separatrix, and core plasma follows 2 to 5 ms later. The reduction in $\tilde{n}_e$ is always followed by changes in the PDF structure; the $\tilde{\bar{v}}_\perp$ consistently shifts from positive to negative values following the L-H-mode-like transitions. The most significant changes in $\tilde{\bar{v}}_\perp$ PDF structure are observed in the region of location of the $\bar{v}_\perp$ minimum. Further evidence of the spatially localised nature of self-regulation between the turbulence level and $\bar{v}_\perp$ is provided from information geometry analysis. Similar observations are presented as the ETB collapses, indicating symmetry in the forward and reverse processes.

1. Introduction

The controlled entry into and exit from the high confinement mode (H-mode) remains a significant area of global fusion research due to its desirability as an operational scenario for future fusion devices such as the International Thermonuclear Experimental Reactor (ITER) [1, 2] and the Spherical Tokamak for Energy Production (STEP) [3].

The external transport barrier's (ETB) complex and non-linear nature, coupled with very fast dynamics, has meant that developing a robust theoretical and predictive model of the L-H transition has yet to be comprehensively established. Through extensive theoretical and more recent experimental studies on conventional aspect ratio tokamaks, it is now widely acknowledged that the dithering L-H transition is governed by the synergistic interaction between plasma turbulence, zonal flows (ZF), and the equilibrium $E \times B$ plasma velocity, $v_{E\times B}$ flow shear [4, 5, 6, 7, 8]. Turbulent transport in plasmas is driven by micro-instabilities, which are severely detrimental to the performance of tokamaks due to the significant removal of heat and particles from the core region. ZFs describe the local movement of the plasma driven by Reynolds stresses through the momentum redistribution of turbulent flows, which leads to a self-regulating process of shear-induced turbulence suppression. The radial pedestal ion pressure gradient drives the $v_{E\times B}$ shear and is essential for turbulence decorrelation through the breakdown of eddies. This mechanism establishes the ETB within a narrow plasma layer just inside the separatrix, significantly reducing the transfer of particles and heat from the confined plasma into the SOL.

Turbulence diagnostics, such as Doppler backscattering (DBS) and beam emission spectroscopy (BES), have played a significant role in the experimental study of turbulence dynamics across confinement transitions on conventional tokamaks [9], with a more limited number of studies performed on low-aspect-ratio machines [10]. In 2023, a newly installed DBS system on MAST-Upgrade (MAST-U) yielded its initial results [11, 12]. This letter presents the first statistical analysis of MAST-U DBS measurements to investigate ETB plasma dynamics over an L-mode to dithering phase to L-mode transition. Since the ETB forms and collapses cyclically over the dithering phase limit cycle oscillations (LCO), it provides an extended period over which the contributing variables and their correlation are studied. This work focuses on DBS measured relative density fluctuations, $\tilde{n}_e$, and perpendicular flow velocity, $\tilde{v}_\perp$. These variables are described using probability density functions (PDFs) as the L-H transition has been consistently shown to generate strongly non-Gaussian distributions [13, 14, 15, 16]. Furthermore, the time evolution of these PDFs is analysed using information geometry, a stochastic method that enables a statistical comparison between the contributing variables via dimensionless quantities. This method is used to calculate the rate of change and the total number of statistical states of these fluctuating variables to investigate their causal relationship.

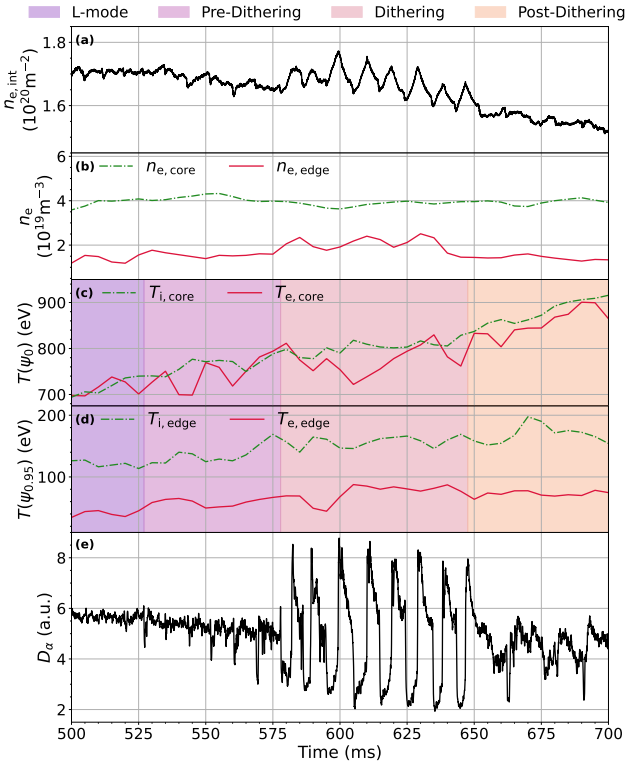

Figure 1. **(a)** core plasma line-integrated n_e, **(b)** core and edge plasma n_e, **(c)** core T_e and T_i measured at $\Psi_N = 0$, **(d)** edge T_e and T_i measured at $\Psi_N = 0.95$, **(e)** D_α intensity over the pre-dithering, dithering, and post dithering phases.

2. Experiment

An NBI-heated MAST-U plasma with a Super-X divertor configuration [17], #48004, was chosen for this investigation. The plasma was initially heated by an off-axis (SW) neutral beam injection (NBI) for 300 ms, $P_{\mathrm{NBI}}^{\mathrm{SW}} = 1.46$ MW, before the dithering phase was triggered by heating from on-axis (SS) NBI, $P_{\mathrm{NBI}}^{\mathrm{SS}} = 0.70$ MW. This input power was sufficiently above the L-H power threshold with a plasma current, $I_{\mathrm{p}} = 750$ kA, toroidal magnetic field, $B_\phi = 0.6$ T. Additional edge plasma power was supplied from sawtoothing phenomena driven by core plasma instabilities. The time-traces of I_{p} and B_ϕ along with the other general plasma parameters such as the NBI power, ohmic power, P_{OHM}, core-radiated power, $P_{\mathrm{core,rad}}$, core and edge plasma electron density, $n_{\mathrm{e}}^{\mathrm{core}}$ and $n_{\mathrm{e}}^{\mathrm{edge}}$, are shown in Figure A1 in Appendix A.

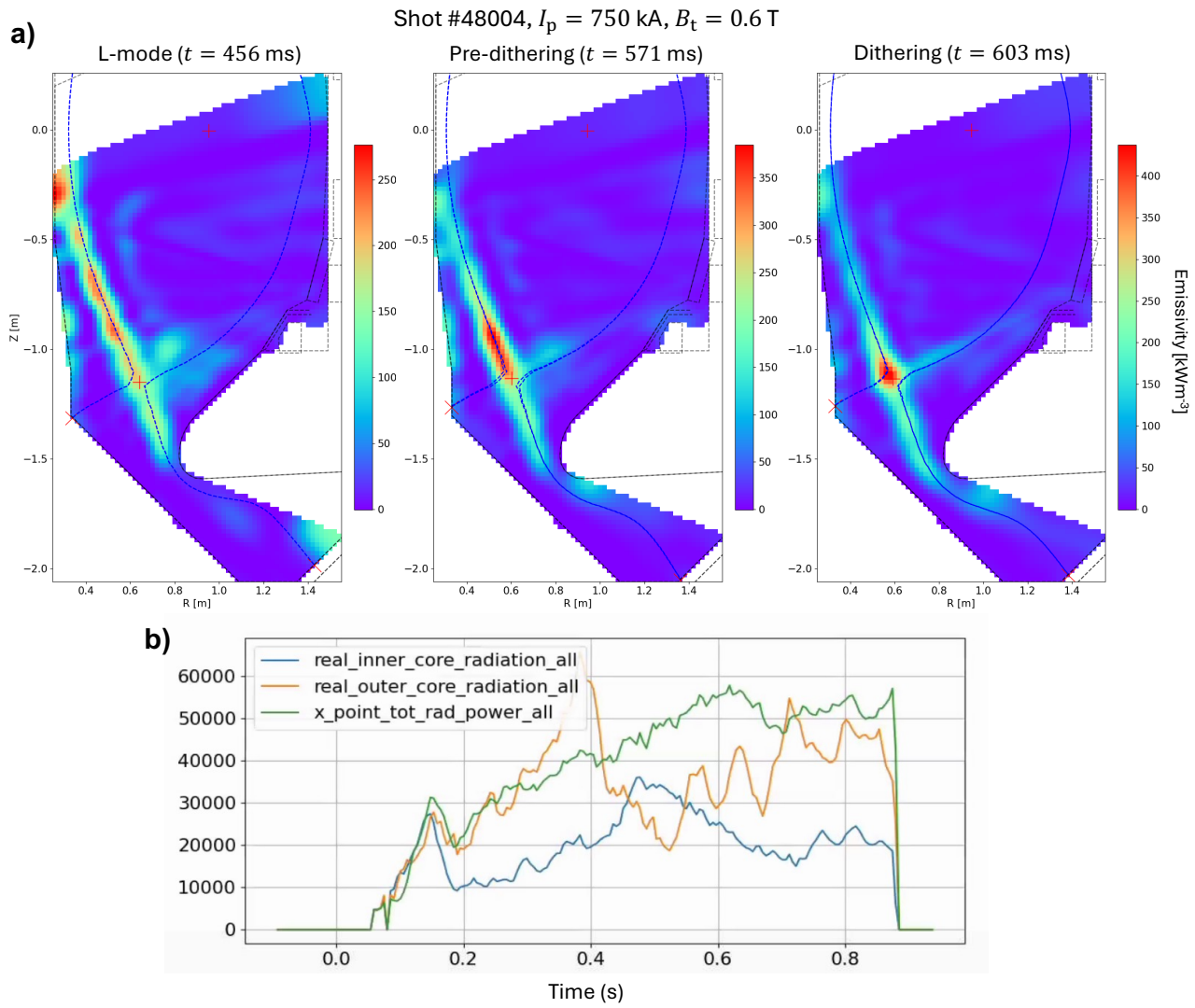

Figure 2. a) Time evolution of the emissivity distribution for Super-X divertor over the L-mode, pre-dithering, and dithering phases for shot #48004. Both inner and outer targets are radiatively detached during the dithering phase and the radiation is localised at the X-point. **b)** The time evolution of the radiation at the inner and outer core, and at the X-point.

The dithering phase for this shot is characterised by well-defined LCOs, which have signature oscillations in the core plasma line integrated n_e^{int} and divertor D_α intensity between t = 578 ms and 648 ms shown by the time traces in Figure 1(a) and (e) and Figure A1(c) and (g). The vertical dashed lines and pink shaded region in Figure 1 indicate the 70 ms dithering phase time window analysed in this study. Figure 1 also shows the L-mode, pre-dithering, and post-dither phases, shaded in purple, pink, and, orange, respectively. These earlier phases show weaker and shallower D_α oscillations triggered by the sawteeth instabilities present throughout this shot. The time evolution of the divertor plasma emissivity 2D reconstruction in Figure 2 shows that both the inner and outer divertor targets were detached by the start of the dithering phase. The radiation is initially distributed along the inner separatrix during the L-mode before localising at the magnetic null point at the beginning of the dithering phase. The radiation zone time traces in Figure 2 (b) show that the X-point radiation remains spatially localised throughout the dithering phase. The resultant localised energy dissipation at the magnetic null potentially contributes to the formation of the dithering phase ETB as it is understood to modify convective patterns close to the separatrix, increasing the flow shear as turbulent eddies are advected. The plasma is thought to self-organise to form the ETB due to an expanding region of locally produced turbulent eddies, which spread further into the edge and core plasma due to the pressure gradient [18].

The n_e^{int} measured by the CO_2/HeNe interferometer [19] has sufficient time resolution to track the sharp increases in the core plasma following the formation of

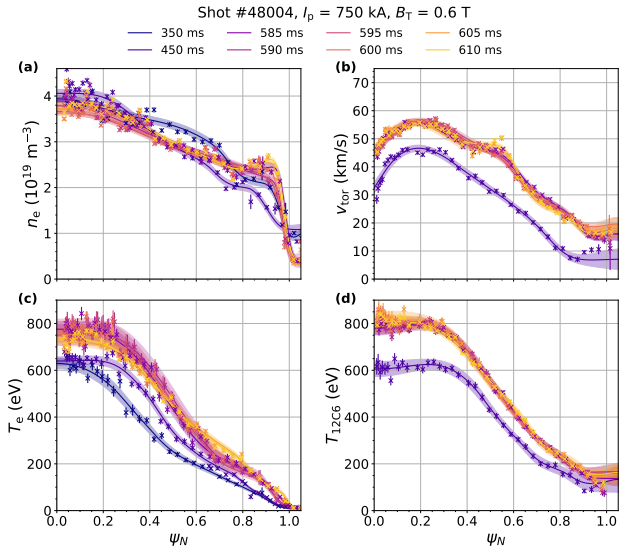

Figure 3. Radial profiles for n_e, T_e, T_i and v_ϕ over L-mode and H-mode like phase of the first LCO for shot 48004.

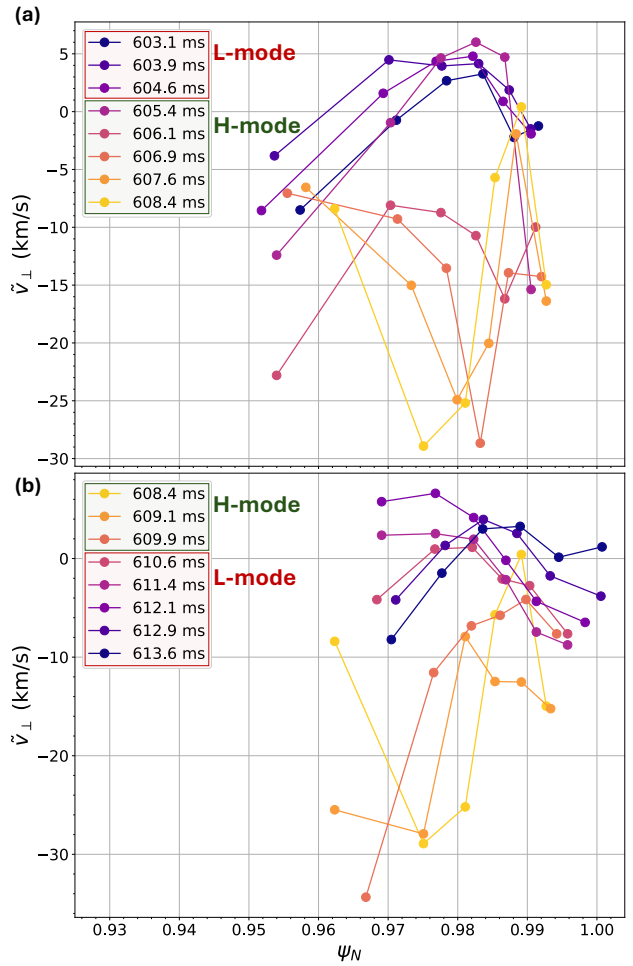

Figure 4. Time evolution of the $\tilde{v}_\perp$ radial profile between t = 603.1-613.6 ms over an **a)** L-H-mode-like and **b)** H-L-mode-like transition in the dithering phase.

the ETB at the start of each LCO, corresponding to the sharp drops in divertor D_α. During the dithering phase, significant n_e, and electron temperature, T_e, gradients are measured with the Thomson Scattering diagnostic (TS) [20] just inside the separatrix ($\psi_N \approx 0.970 - 0.990$), shown in Figure 1 (b), (c) and (d). The carbon ion, (C^{6+}), temperature, T_i, measured with charge exchange spectroscopy (CXRS) [17], is the same as T_e in the core plasma and $T_i^{edge} = 1.5T_e^{edge}$ in the plasma edge. The length of each LCO is observed to increase over time; the H-mode-like stage of the first dither lasts approximately 3.5 ms, followed by two L-H-mode-like cycles of approximately 7 ms, with subsequent cycles progressing to 10 ms duration.

The radial n_e, T_e, T_i and C^{6+} toroidal velocity profiles are shown in Figure 3 with fits generated by the OMFITprofiles module [21]. In the plasma region within the last closed flux surface (LCFS), ψ_N = 0.92-0.94, the T_e and T_i profiles are approximately 60 eV cooler in the L-mode (t = 350 and t = 450), n_e exhibits shallower gradients, and v_{tor} is approximately 10 kms^{-1} lower than in the dithering phase between t = 585 and t = 610 ms. The most significant contribution to the pedestal pressure gradient in the H-mode-like phase of the LCOs is from n_e, with steep gradients and a clear pedestal knee forming at ψ_N = 0.92-0.94, with $n_e^{knee} = 2.14\text{-}2.61\times10^{19}$ m^{-3}.

Figure 4 (a) shows the progression of the $\tilde{v}_\perp$ radial profile structure from the L-mode 1.5 ms before the L-dithering phase transition, and subsequently over 3.8 ms of the first LCO. Figure 4 (b) shows the progression of the reverse process. For the forward transition, the minimum in $\tilde{v}_\perp$ is first seen at ψ_N = 0.987 (channel 2) at t = 606.1 ms at and then progresses to ψ_N = 0.975 in channel 5, at t = 608.4 ms. The minimum in $\tilde{v}_\perp^{min}$ corresponds to the radial location of the electric field minimum, E_r^{min}, and the steepest gradient regions of ∇E_r and $\nabla\tilde{v}_\perp$ on either side [14, 22]. Before the back transition occurs at 610.0 ms, there is already significant degradation of the E_r well structure, which is seen to also propagate inwards from the edge plasma.

3. Information Geometry

Information geometry is a stochastic method which quantifies the relative change between variable distribution functions. The change in the number of statistical states between two PDFs is calculated via dimensionless quantities to enable the comparison and correlation of different variables. The studies by [13, 24] first applied information geometry to study the self-regulatory behaviour of phase transitions for simulated (numerically calculated) magnetically confined fusion plasma variables.

It is assumed that the variables being considered

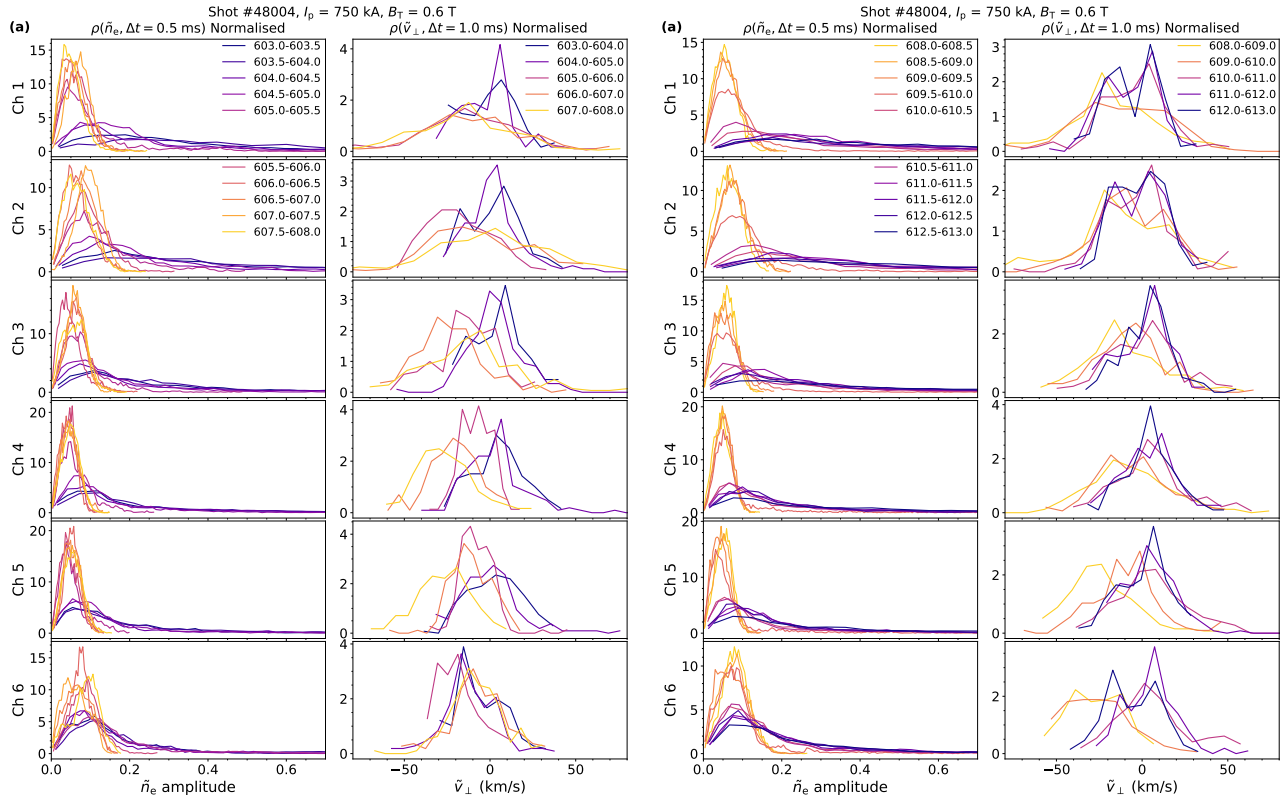

Figure 5. $\tilde{n}_e$ and $\tilde{v}_\perp$ PDF evolution over **(a)** L-H transition $575 \leq t \leq 580$ ms and **(b)** H-L transition $580 \leq t \leq 585$ ms.

are stochastic and can be mathematically described by a time-dependent PDF $\rho(x,t)$. The information rate, $\Gamma(t)$, is the rate of change in the number of statistical states between two temporally adjacent PDFs $\rho(x,t)$ and $\rho(x,t+\delta t)$ and defined as [14, 15, 16]:

$$\Gamma(t) = \sqrt{\int dx \frac{1}{\rho(x,t)} \left[\frac{\partial \rho(x,t)}{\partial t}\right]^2}. \quad (1)$$

The information length, $\mathcal{L}(t)$, is the total number of distinct statistical states that a stochastic variable x passes through between $t = 0$ and t and is calculated by:

$$\mathcal{L}(t) = \int_0^t \Gamma(t')dt'. \quad (2)$$

A large information rate indicates that the number of statistical states between two PDFs has changed significantly [13, 24]. Physically, this could be interpreted as a variable that is volatile, turbulent, or rapidly undergoing phase transitions that are changing its properties.

4. Results

The $\tilde{n}_e$ and $\tilde{v}_\perp$ data are discretised into probability density functions (PDF) [14, 15, 16] and shown for six DBS channels in Figure 5. This 10 ms time window covers the (a) L-H-mode-like transition and (b) H-L-mode-like transition of one LCO starting at t = 575 ms, using time PDF intervals of $\Delta t^{n_e}_{\text{PDF}} = 0.5$ ms and $\Delta t^{v_\perp}_{\text{PDF}} = 1.0$ ms.

4.1. PDF evolution over the LCO forward transition

The suppression of turbulence manifests as the progression from asymmetric and tailed distributions to more Gaussian-like. In Figure 5, this first occurs for the 605.0-605.5 ms PDF and the reduction in asymmetry and tailedness is most significant in the region $0.970 \leq \psi_N \leq 0.978$ (channels 4 and 5). Similar evolutions in the neighbouring regions, namely channels 1-3 and 6, are observed at later times but do not experience suppression to the same extent. However, at the time of this PDF, the profile in 4 at 605.4 indicates that the E_r well is yet to be established. This highlights that the turbulence suppression through the reduction in $\tilde{n}_e$ precedes the formation of the E_r well, which drives sheared $E \times B$ flows that assist in sustaining the ETB. This phase lag between turbulence level and perpendicular velocity agrees with the L-H transition predator-prey model by Kim et al. [4], and spatially further in than similar experimental observations on DIII-D [7].

Similarly, the greatest changes in the $\tilde{v}_\perp$, are also observed across $0.970 \leq \psi_N \leq 0.978$ (channels 4 and

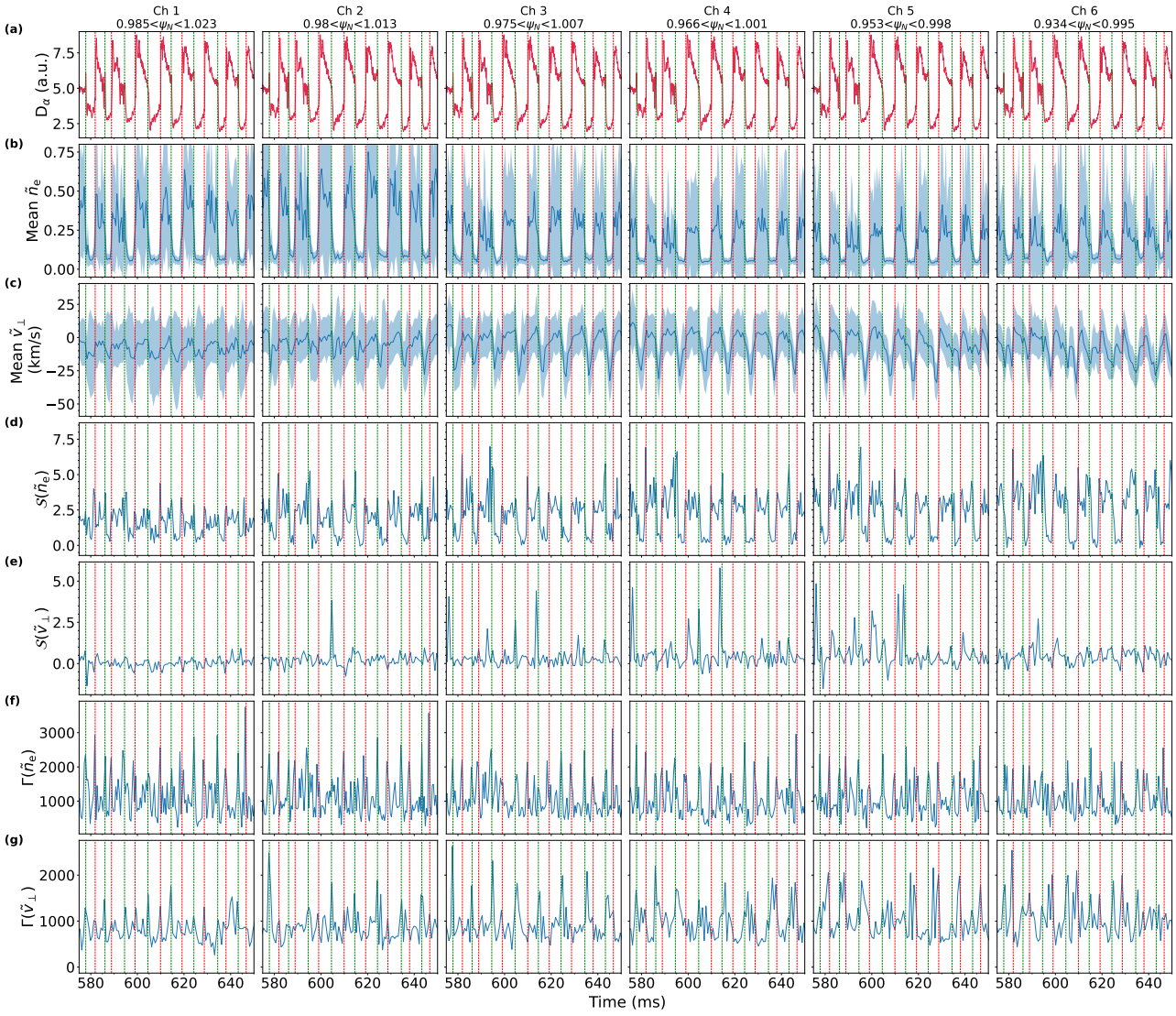

Figure 6. Time evolution of the **a)** D_α radiation, **b)** $\tilde{n}_e$, **c)** $\tilde{v}_\perp$, **d)** $\mathcal{S}_{\tilde{n}_e}$, **e)** $\mathcal{S}_{\tilde{v}_\perp}$, **f)** $\Gamma_{\tilde{n}_e}$, and **g)** $\Gamma_{\tilde{v}_\perp}$ over the dithering phase.

5) in figure 5, where the inner $\nabla\ \tilde{v}_\perp$ develops. For all channels, there is a shift from more positive values of $\tilde{v}_\perp$ in the L-mode to negative values in the H-mode. However, there is a notable difference in the evolution of the PDF structure for the inner and outer channels. The edge channels 1-2 progress from relatively narrow in the L-mode to heavy-tailed distributions in the H-mode. The tailedness of the PDFs in H-mode for channels further becomes comparable to the L-mode PDFs.

4.2. PDF evolution over the LCO back transition

The PDF evolution as the ETB degrades over the H-L-mode-like transition of the LCO is presented in Figure 5(b) for $\tilde{n}_\mathrm{e}$ and $\tilde{v}_\perp$. The reverse process of the L-H-mode-like transition is observed: the $\tilde{n}_\mathrm{e}$ PDFs progress from narrower and more symmetric distributions to much broader, asymmetric, and heavily tailed distributions. The first indication of the back transition PDF progression is observed in channels 1 and 2 at t = 609.5-610.0 ms, before the increase in D_α intensity. Significant changes in the $\tilde{v}_\perp$ PDFs are similarly observed in the back transition. The progression of the $\tilde{v}_\perp$ PDFs from narrow to shallow distributions in Figure 5 (a) is initially observed in channels 3-5 for t = 608.0-609.0 and t = 609.0-610.0 ms. This precedes a significant shift back to narrower distributions and more from negative to positive $\bar{\tilde{v}}_\perp$. The $\tilde{v}_\perp$ profile evolution seen in figure 4, indicates that the formation of the E_r well structure that causes the H-mode-like PDFs to become significantly shallower and heavily tailed.

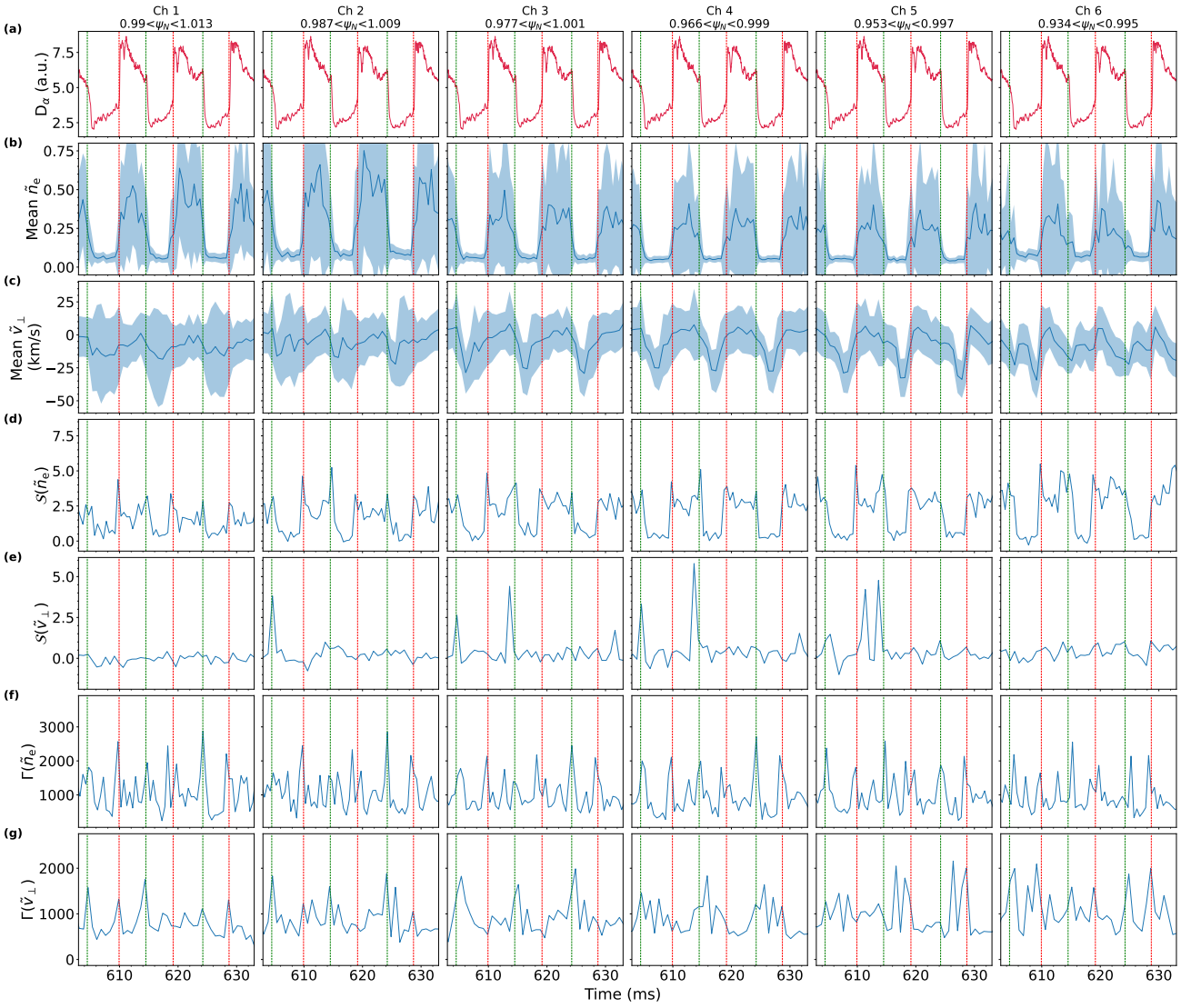

Figure 7. Time evolution of the **a)** D_α radiation, **b)** $\tilde{n}_e$, **c)** $\tilde{v}_\perp$, **d)** $\mathcal{S}_{\tilde{n}_e}$, **e)** $\mathcal{S}_{\tilde{v}_\perp}$, **f)** $\Gamma_{\tilde{n}_e}$, and **g)** $\Gamma_{\tilde{v}_\perp}$ over two L-H and H-L transitions.

4.3. Statistical analysis

Figures 6 and 7 show the diverter D_α intensity, mean fluctuations, $\bar{\tilde{n}}_e$ and $\bar{\tilde{v}}_\perp$, standard deviations, $\sigma_{\tilde{n}_e}$ and $\sigma_{\tilde{n}_\perp}$, skewnesses, $S_{\tilde{n}_e}$ and $S_{\tilde{v}_\perp}$, and information rates, $\Gamma_{\tilde{v}_e}$ and $\Gamma_{\tilde{v}_\perp}$. There is a substantial decrease in $\bar{\tilde{n}}_e$ and $\sigma_{\tilde{n}_e}$ across all channels in the H-mode-like phases of all LCOs. The difference in $\bar{\tilde{n}}_e$ between the L-mode-like and H-mode-like phases generally increases from channel 1 to 6 (edge to core). As discussed in Section 4.1, the decrease in $\bar{\tilde{n}}_e$ first occurs across ($0.970 \leq \psi_N \leq 0.978$) (channels 4-5) with the other channels lagging behind by 1-2 ms. This region corresponds to the inner and outer $\tilde{v}_\perp$ shear layer either side of $\tilde{v}_\perp^{\min}$ and the steep ∇P_e illustrated in figures 3 and 4. Spikes in the $\Gamma_{\tilde{n}_e}$ coincide with both the forward (green vertical lines) L-H-mode-like transitions and reverse (red vertical lines) across the entire region examined in this study (channels 1-6) and shown in Figures 6(f) and 7(f). These results indicate that the rapid changes in the $\tilde{n}_e$ PDF characteristics occur at the transition into and out of the H-mode-like phase of the LCOs. The maximum negative mean $\tilde{v}_\perp$ values in the steep pedestal gradient region (channels 3-5) consistently lag behind the $\tilde{n}_e$ peak by 1-3 ms. This phase lag between the turbulence level and the perpendicular velocity is thought to be due to the generation of zonal flows by turbulence mentioned earlier, and in agreement with previous experimental observations on DIII-D [7, 14, 15, 16].

Following the initial changes in $\bar{\tilde{n}}_e$, the values of $\bar{\tilde{v}}_\perp$ increases in the negative direction. Channels 3-5 experience a more significant difference in $\bar{\tilde{v}}_\perp$ and $\sigma_{\tilde{n}_\perp}$ on average across the LCOs (5.7 to -33.5 kms^{-1}) than channels 1-2 (1.2 to -18.4 kms^{-1}) and channel 6 (5.5 to

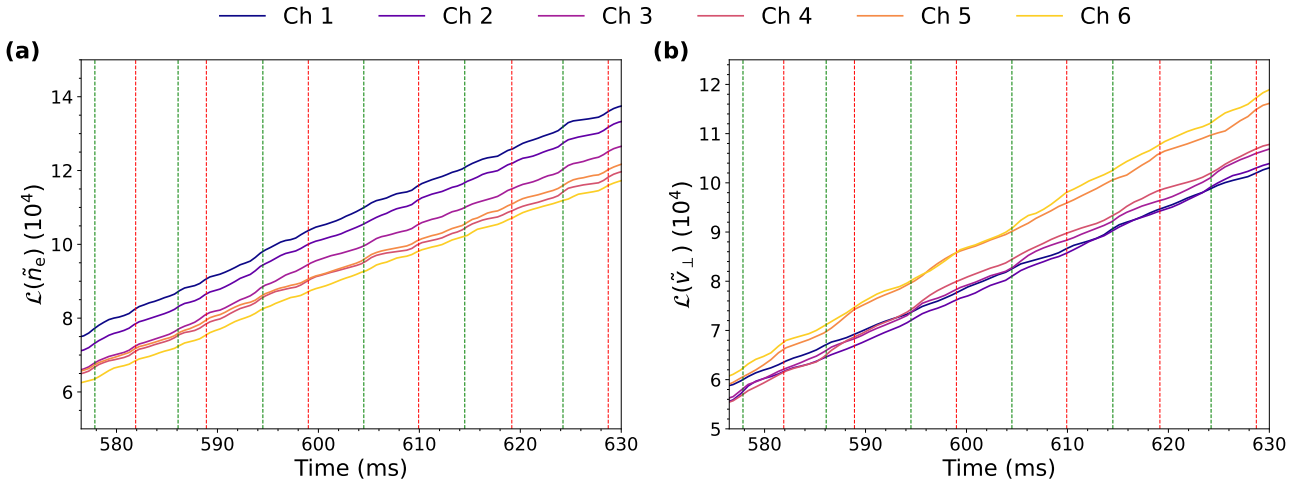

Figure 8. Time evolution of the information lengths for **a)** $\mathcal{L}_{\tilde{n}_e}$ and **b)** $\mathcal{L}_{\tilde{v}_\perp}$ over two L-H and H-L transitions.

- 19.6 kms^{-1}), seen in figures A1 and 1(c). The time trace of $\Gamma_{\tilde{v}_\perp}$ in Figures A1 and 1 peak at the L-H-mode-like transitions for channels 1 and 2 but tend to lag for channels 3,4,5, and 6 by approximately 1-3 ms. In contrast to $\Gamma_{\tilde{n}_e}$, $\Gamma_{\tilde{v}_\perp}$ does not peak at or following the H-L-mode-like transitions. No correlation of changes in $\mathcal{S}_{\tilde{v}_\perp}$ with the start or end of the LCOs is apparent in Figures A1 and 1(e).

As the pedestal pressure increases in the H-mode-like phases of the LCOs, the diamagnetic component of the mean plasma poloidal velocity flow increases, zonal flows decrease due to $\tilde{n}_e$, and the $\bar{\tilde{v}}_\perp$ shifts to negative values shown in Figures 6 and 7(c) and (e). The resulting sheared velocity flow appears to be insufficient to maintain the H-mode-like phase as the plasma transitions back to the L-mode-like phase and $\bar{\tilde{v}}_\perp$ can be seen to decrease from the maximum negative value before each H-L-mode-like transition (red vertical lines) for channels 3 to 5 in Figures 6 and 7. For these channels, the PDF width, indicated by $\sigma_{\tilde{v}_\perp}$, decreases from approximately 20 kms^{-1} in the L-mode like phases to 15 kms^{-1} in the H-mode like phases.

Figure 8 shows the information lengths of the density and perpendicular flow fluctuations, $\mathcal{L}_{\tilde{n}_e}$ and $\mathcal{L}_{\tilde{v}_\perp}$. For $\mathcal{L}_{\tilde{n}_e}$ in Figure 8(a), channels 3,4, and 5 are the most strongly correlated over the first two LCOs of the dithering phase. However, from the third LCO, channel 3 separates, leaving channels 4 and 5 closely coupled in terms of statistical states. Therefore, the driving mechanism for the density fluctuations in channels 4 and 5 remains the same throughout the dithering phase. A similar examination of $\mathcal{L}_{\tilde{v}_\perp}$ in Figure 8(b) shows the formation of three distinct regions of $\tilde{v}_\perp$ statistical states after the second LCO, corresponding to channels 1-2, 3-4 and 5-6. It is interesting to note that these do not overlap directly with the $\mathcal{L}_{\tilde{n}_e}$ regions, indicating different or additional driving $\tilde{v}_\perp$ mechanism to turbulence as the dithering phase progresses beyond the first two LCOs, such as the mean flow velocity driven by the diamagnetic term.

5. Conclusion

Experimental evidence is presented regarding the role of zonal flows in suppressing plasma density fluctuations in the pedestal region corresponding to the minimum in $\tilde{v}_\perp$ within the confined plasma on MAST-U. The start of the dithering phase is preceded by the spatial localisation of energy dissipation at the magnetic null point. The edge pressure gradient increases following the initial formation of the ETB at the start of LCO, increasing the diamagnetic component of the measured $\tilde{v}_\perp$. From the analysis of the $\tilde{n}_e$ PDFs, the turbulence suppression is first observed in a narrow region ($0.970 \leq \psi_N \leq 0.978$) and precedes the formation of the $\tilde{v}_\perp$ well by approximately 2-3 ms. The consequences of this structure are heavily tailed $\tilde{v}_\perp$ PDFs. Sharp spikes in the measured $\Gamma_{\tilde{n}_e}$ consistently coincide with the forward and backwards transitions of the LCO, indicating abrupt changes in the PDF structures. In contrast, sudden changes in $\Gamma_{\tilde{v}_\perp}$ are only observed close to or following the forward LCO transitions. Information length analysis reveals channels 3-5 are strongly correlated in $\tilde{n}_e$ statistical space at the start of the dithering phase, which reduces to a region channels 4-5 as the LCOs progress. The $\mathcal{L}_{\tilde{v}_\perp}$ time trace reveals the formation of three distinct regions of $\tilde{v}_\perp$ statistical space after the second LCO across the pedestal region decoupled from the $\mathcal{L}_{\tilde{n}_e}$ regions. This result indicates that mechanisms additional to turbulence drive $\tilde{v}_\perp$ as the dithering phase evolves.

6. Acknowledgment

This work has been (part-) funded by the EPSRC Energy Programme [grant number EP/W006839/1

7. References

[1] E.J. Doyle, *et al.*, (2007) Nucl. Fusion **47** S18
[2] A. Loarte, *et al.*, (2021) Nucl. Fusion **61** 076012
[3] M. Lenholm, *et al.*, Nucl. Fusion **64** 096036 (2024)
[4] E. J. Kim and P. H. Diamond,(2003) Phys. Rev. Lett. **90**, 185006
[5] P. H. Diamond, *et al.*, (2005) Plasma Phys. Controlled Fusion **47**, R35
[6] A. Fujisawa, *et al.* (2009) Nucl. Fusion **49**, 013001
[7] L. Schmitz *et al.*, (2012)Phys. Rev. Lett. **108**, 155002
[8] K. H. Burrell, (2020) Phys. Plasmas **27**, 060501
[9] M. Berta *et al*, (2015) Fusion Engineering and Design, **96–97**
[10] A. R. Field *et al.*, (2012) Rev. Sci. Instrum, **83**, 013508
[11] T. L. Rhodes, *et al.*, (2022) Rev. Sci. Instrum. **93**, 113549
[12] P. Shi, *et al.*, (2023) JINST **18** C11022
[13] R. Hollerback, *et al.*, (2020) Phys. Plasmas **27**, 102301
[14] H. J. Farre-Kaga, *et al.*, (2023) EPL **142** 64001
[15] Y. Andrew, *et al.*, PPCF (2024) **66** 055009
[16] T. Ashton-Key, *et al*, (2025) Plasma Phys. Control. Fusion
[17] J. Harrison, *et al.*, 2024 Nuc. Fusion **64** 112017
[18] G. Dif-Pradalier, *et al.*, 2022 Commun. Phys. **5** 229
[19] G.L. Derks, *et al.*, (2024) Fusion Eng. and Design **(**202) 114387
[20] J.G. Clark, *et al.*, (2022) Rev. Sci. Instrum. 93, 103534
[21] N. Logan, *et al.*, (2018) Fusion Science and Technology, **74**
[22] Q. Pratt, *et al.*, (2022) Plasma Phys. Control. Fusion **64** 095017
[23] Q. Pratt, *et al.*, (2025) Fusion Science and Technology 1-23
[24] E. Kim and R. Hollerbach, (2020) Phys. Rev. Research **2**, 023077 (2020)

Appendix A. Full Time Trace Data

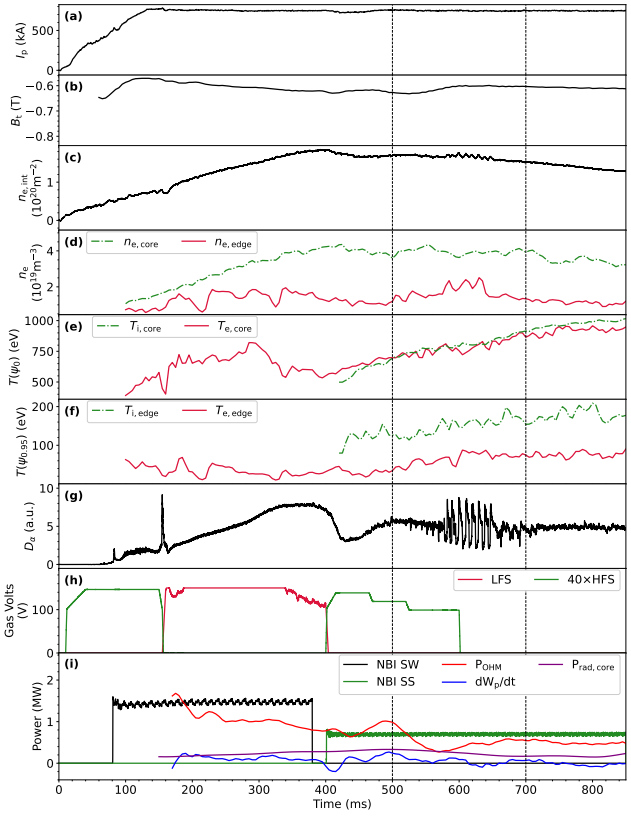

Figure A1. Time trace data for shot #48004. **(a)** plasma current with $I_p = 750$ kA flat-top, **(b)** toroidal magnetic field, $B_\phi \approx -0.6$ T (opposite direction to I_p), **(c)** core line integrated electron density n_e, **(d)** core and edge n_e, **(e)** core T_e and T_i, **(f)** edge T_e and T_i, **(g)** D_α intensity, **(h)** gas fuelling voltages on the high-field and low-field sides, and **(i)** power parameters, including NBI input power for off-axis (SW) and on-axis (SS) NBI, ohmic power, core radiated power, and rate of change of stored plasma energy. Vertical black dashed lines correspond to the time window of interest, shown in Figure 1.